Alkali-earth metal bridges formed in biofilm matrices regulate the uptake of fluoroquinolone antibiotics and protect against bacterial apoptosis

Environmental Pollution xxx (2016) 1–12

Contents lists available at ScienceDirect

Environmental Pollution

journal homepage: www.elsevier.com/locate/envpol

Alkali–earth metal bridges formed in biofilm matrices regulate the uptake of fluoroquinolone antibiotics and protect against bacterial apoptosis☆

Fuxing Kang [a], Qian Wang [b], Weijun Shou [a], Chris D. Collins [c], Yanzheng Gao [a, *]

[a] Institute of Organic Contaminant Control and Soil Remediation, College of Resources and Environmental Sciences, Nanjing Agricultural University, Jiangsu 210095, China
[b] State Key Laboratory of Lake Science and Environment, Nanjing Institute of Geography and Limnology, Chinese Academy of Sciences, Jiangsu 210008, China
[c] Soil Research Centre, University of Reading, Whiteknights, Reading RG6 6DW, UK

ARTICLE INFO

Article history:
Received 6 July 2016
Received in revised form
6 September 2016
Accepted 11 September 2016
Available online xxx

Keywords:
Fluoroquinolone antibiotics
Biofilms
Alkali–earth metals
Bridging energy
Computational chemistry
Escherichia coli

ABSTRACT

Bacterially extracellular biofilms play a critical role in relieving toxicity of fluoroquinolone antibiotic (FQA) pollutants, yet it is unclear whether antibiotic attack may be defused by a bacterial one-two punch strategy associated with metal-reinforced detoxification efficiency. Our findings help to assign functions to specific structural features of biofilms, as they strongly imply a molecularly regulated mechanism by which freely accessed alkali–earth metals in natural waters affect the cellular uptake of FQAs at the water-biofilm interface. Specifically, formation of alkali-earth-metal (Ca^{2+} or Mg^{2+}) bridge between modeling ciprofloxacin and biofilms of *Escherichia coli* regulates the trans-biofilm transport rate of FQAs towards cells (135-nm-thick biofilm). As the addition of Ca^{2+} and Mg^{2+} (0–3.5 mmol/L, CIP: 1.25 μmol/L), the transport rates were reduced to 52.4% and 63.0%, respectively. Computational chemistry analysis further demonstrated a deprotonated carboxyl in the tryptophan residues of biofilms acted as a major bridge site, of which one side is a metal and the other is a metal girder jointly connected to the carboxyl and carbonyl of a FQA. The bacterial growth rate depends on the bridging energy at anchoring site, which underlines the environmental importance of metal bridge formed in biofilm matrices in bacterially antibiotic resistance.

1. Introduction

More and more attention has been paid to the challenging issue on environmental contamination of antibiotics in recent years (Martinez, 2009; Pruden et al., 2006). A nationwide survey of pharmaceutical compounds from USA showed that a number of antibiotics were detected in 27% of 139 rivers at concentrations up to 0.7 μg/L (Kolpin et al., 2002). And the annual usage of antibiotics has been estimated to be between 1.0×10^5 and 2.0×10^5 tons globally, with more than 2.5×10^4 tons used each year in China (Xu et al., 2007). The cellular uptake of antibiotics via trans-biofilm transport will inevitably increase the risk of microbial death, ecological disruption, amplification of antibiotic resistance genes and even the creation of "superbugs" (Desnottes and Diallo, 1992; Pruden et al., 2013). However, regulated mechanism occurring at water-biofilm interface, by which bacteria exert extracellular biofilm barrier to defuse the antibiotic stress, has not been well understand. This process has profound consequences for environmental stability.

Fluoroquinolone antibiotics (FQAs), which comprise an important and hard-degradable class of synthetic pharmaceuticals, have been widely used and have been introduced into the environment by a multitude of human and veterinary activities over the last 30 years in Europe and the United States (Baquero et al., 2008; Mompelat et al., 2009). Bacteria generally hide into a biofilm matrix to deal with the presence of these synthetic antibiotics (Wingender et al., 2012). One component of the so-called bacterial one-two punch strategy is to use an extracellular biofilm permeability barrier to impede the cellular uptake of antibiotic stressors. Such physical defenses in response to antibiotics might be

☆ This paper has been recommended for acceptance by Baoshan Xing.

* Corresponding author.
E-mail addresses: gaoyanzheng@njau.edu.cn, gaosoil@163.com (Y. Gao).

http://dx.doi.org/10.1016/j.envpol.2016.09.029
0269-7491/

inefficient and energetically very costly (Martínez et al., 2007; Rice, 2006). For example, previous studies have shown that sorption of FQAs to oxygen- and nitrogen-containing dissolved organic matter (DOM) displays a nonlinear saturation pattern (with a Freundlich exponent $n = 0.40–0.51$) (Zhang et al., 2012), whereas their affinity to phospholipids exhibits a linear partitioning pattern (partitioning coefficient = 20.0–79.4 L/kg) (Merino et al., 2002, 2003). These findings implies that biofilms containing similar oxygen and nitrogen groups have a relatively low capacity (Walter, 2012) to absorb FQAs and may result in high intracellular uptake due to the low-efficiency of extracellular FQA interception. Furthermore, extracellular accretions that act as entrapment agents will be energetically very costly, considering the demand for major saccharide and protein moieties during the formation of biofilms. Nevertheless, little information is currently available to determine how bacteria efficiently and economically deal with such stressors; this issue requires proper investigation.

A positively charged metal bridging connection between electronegative biofilms and negatively charged FQAs (i.e., their functional groups) may be the other component of the one-two punch strategy for defending against antibiotic attack. Given the strong electrostatic attraction between electronegative biofilms/FQAs and accessible alkali–earth metals, the formation of a stable structure would anchor the FQAs in biofilms via a metal bridge. Whereas one side of the metal-to-FQA connection (metal–carbonyl interaction) is supposedly understood (Aristilde and Sposito, 2008), attractions between metals and extracellular biofilm components on the other side are more multifarious and complicated. Thus, a quantitative description of an alkali–earth–metal bridge based on these weak attractions is crucial for quantitatively expounding the association of such weak interactions at the molecular level. Generally, on the basis of spectroscopic data, it is considered that alcohol, carboxyl, phosphoric, and amino-acid residue groups in biofilm matrices may be involved in interactions with such metals as Zn^{2+}, Co^{2+}, and Ca^{2+} (Ha et al., 2010; Sun et al., 2009; Sundararajan et al., 2011; Xiong et al., 2002). These results only suggest that biofilms may utilize their electronegative groups to interact with metals, but not know whether antibiotic attack may be defused by a metal-reinforced detoxification efficiency occurring at water-biofilm interface. And these spectroscopic data should be considered qualitative, as they do not specify which of the functional groups in biofilms are involved in metal binding. The listed spectroscopic techniques have been unable to access quantitative descriptions of imperceptibly weak interactions at the microscopic level. Therefore, based on the idea that FQA–biofilm interaction occurs via a metal bridge, including bridging energy and spectroscopic analyses, multiple approaches are necessary to substantiate an association between alkali–earth metals and the extracellular retardation of FQAs and biological growth.

In the present study, we investigated the association of bacterial extracellular biofilms with FQAs via an alkali–earth–Ca^{2+}/Mg^{2+} bridge and determined the influence of metal bridges in biofilms on the extracellular interception and cellular uptake of FQAs. *In situ* confocal laser scanning microscopy (CLSM), X-ray photoelectron spectroscopy (XPS), Fourier transform infrared spectroscopy (FTIR), and ^{13}C nuclear magnetic resonance (^{13}C NMR) were used to confirm the formation of alkali–earth–metal bridges in biofilms. A series of batch experiments was performed to explore the effect of alkali–earth–metal bridges in biofilm matrices on extracellular interception, trans-biofilm cellular uptake of a model antibiotic, and bacterial apoptosis. Subsequently, eight FQAs were used to determine the dependence of *E. coli* growth on the bridging energy at major sites through a set of fluorescence microtitration and computational chemistry analyses.

2. Materials and methods

2.1. Materials

Eight fluoroquinolone antibiotics (FQAs, ≥99.0%) were purchased from Sigma-Aldrich Co., Ltd, USA, namely ciprofloxacin (CIP), norfloxacin (NOR), enrofloxacin (ENR), ofloxacin (OFL), lomefloxacin (LOM), levofloxacin (LEV), pefloxacin (PEF), and flerofloxacin (FLE). Their physicochemical properties, including molecular weight (MW), the dissociation constant for carboxyl groups ($pK_{a\text{-}COOH}$), and the octanol–water partition coefficient ($\log K_{ow}$), are listed in **Table S1**. Magnesium sulfate ($MgSO_4 \cdot 7H_2O$, ≥99.0%) and calcium sulfate ($CaSO_4$, ≥99.0%) were purchased from Sinopharm Chemical Reagent Co., Ltd, China. Milli-Q water (18.2 MΩ × cm, Millipore, USA) was used for all experiments.

Other chemicals (as listed below, purity > 99.0%) that were purchased from Nanjing Chemical Reagent Co., Ltd. were used to prepare modified chloride-free culture medium (Kang et al., 2014). The medium contained $K_2HPO_4 \cdot H_2O$ (28 mmol/L), $KH_2PO_4 \cdot 3H_2O$ (2.2 mmol/L), NH_4NO_3 (18.7 mmol/L), $CaSO_4$ (0.001 mmol/L), K_2SO_4 (2.0 mmol/L), $MgSO_4 \cdot 7H_2O$ (1.0 mmol/L), peptone (10 g/L), and a trace element solution (10 mL/L). The trace element solution contained $Na_2EDTA \cdot H_2O$ (5.0 g/L), $Fe_2(SO_4)_3$ (0.37 g/L), ZnO (0.05 g/L), $CuSO_4 \cdot 5H_2O$ (0.015 g/L), $Co(NO_3)_2 \cdot 6H_2O$ (0.01 g/L), $(NH_4)_6Mo_7O_{24} \cdot 4H_2O$ (0.01 g/L), and H_3BO_3 (0.01 g/L). The pH of the medium was adjusted to 7.4 with sulfuric acid (98.0%). When necessary, solid agar medium was prepared with 1 L of chloride-free medium and 15 g of agar powder. The sulfuric acid (0.01 mmol/L H_2SO_4) and sodium hydroxide (0.02 mmol/L NaOH), used for pH adjustment in batch experiment and fluorescence microtitration, were purchased from Nanjing Chemical Reagent Co., Ltd. (Nanshi, China).

2.2. Biofilm manipulation

Our previous method was used to manipulate the extracellular biofilms (Fang et al., 2002; Kang et al., 2014; Liu and Fang, 2002). In brief, *Escherichia coli* (DH5α) was initially cultured in 20 mL of chloride-free medium at 37 °C for a 12-h recovery of growth. The bacterial suspension (5 mL) was then transferred to fresh chloride-free medium (1.0×10^3 mL) and grown for an additional 48 h to reach the stable growth phase. *E. coli* cells were collected by low-speed centrifugation (3×10^3 *g*, 6 min, 4 °C) followed by washing with Milli-Q water to obtain pure, pristine *E. coli* (high-biofilm *E. coli*).

Low-biofilm *E. coli* was obtained by the removal of biofilms from the *E. coli* surface using a sonication/centrifugation procedure (Kang et al., 2014). Specifically, one-half of the (high-biofilm) *E. coli* pellet was suspended to an initial volume of 500 mL and then processed by a low-intensity ultrasonic process for 7.0 min at an intensity of 2.5 W/cm^2 and a frequency of 40 kHz at 4 °C. The *E. coli* suspension was then centrifuged for 20 min at 2.0×10^4 *g* and 4 °C. The settled pellets were collected as low-biofilm *E. coli* samples. The supernatant, which was filtered through a 0.22-μm membrane (Anpel, Shanghai, China), represented an aqueous biofilm solution and was stored at 4 °C for later chemical analyses. Elemental analysis was performed on freeze-dried biofilms using an X-ray photoelectron spectrometer (Thermo Fisher Scientific, Waltham, MA, USA), and the percentage contents of C (38.96), O (29.88), N (30.14), and S (1.02) were determined. The dry weight of the extracted aqueous biofilms (25.7 mg/L) was measured by an oven-drying method (2 h at 105 °C) (Comte et al., 2006). The major proteins (345.1 mg/g) and polysaccharides (173.8 mg/g), and a small quantity of nucleic acid (0.33 mg/g), were measured according to previously reported techniques (Burton, 1956; Dubois

Please cite this article in press as: Kang, F., et al., Alkali–earth metal bridges formed in biofilm matrices regulate the uptake of fluoroquinolone antibiotics and protect against bacterial apoptosis, Environmental Pollution (2016), http://dx.doi.org/10.1016/j.envpol.2016.09.029

et al., 1956; Lowry et al., 1951). The low concentration of nucleic acid in the biofilms indicated negligible cell lysis during the biofilm extraction procedure.

2.3. Interception and uptake of FQA and E. coli apoptosis

High- and low-biofilm *E. coli* cells that were subjected to different biofilm manipulations were suspended in 1.0 L of ultrapure water to obtain approximately 4.0×10^7 cells/mL of each type of *E. coli*. A liquid suspension of bacteria (40 mL) was placed into a 50-mL conical flask equipped with a permeable silica-gel stopper prior to the addition of aqueous alkali–earth–metal stock solutions (200 mmol/L, alkali–earth Ca^{2+} or Mg^{2+}) and an aqueous CIP stock solution (1 mmol/L) to the desired concentrations (metals: 0–3.5 mmol/L; CIP: 1.25 μmol/L). Notably, the concentrations of the added alkali–earth metals were within the range of natural oceanic water (Ca^{2+}: 53.75 mmol/L; Mg^{2+}: 10.1 mmol/L) and fresh water (Ca^{2+}: about 1.75 mmol/L; Mg^{2+}: about 1.77 mmol/L) (Adkins et al., 2002; Bowen, 1979). Here, the added concentration of $CaSO_4$ was far below its solubility limit (14.2–15.4 mmol/L at 10–40 °C) (Harvie et al., 1984). The static suspension experiment was performed in the dark for 4 h at 120 rpm and 37 °C.

A portion of the *E. coli* suspension was used to extract the CIP that was retained in extracellular matrices and absorbed into the cell interiors. The CIP in extracellular matrices was extracted using the biofilm-extraction method described above. The CIP antibiotic was obtained during the separation of biofilms from the *E. coli* surface. For low-biofilm *E. coli*, CIP extraction from extracellular matrices was also performed using the same procedures. Additionally, an ultrasonic method of cellular disruption was used to obtain the intracellular components for CIP antibiotic quantification (Turiel et al., 2006). An *E. coli* sample (5 mL) was subjected to ultrasonic disruption at 450 W and 24 kHz (Φ6, Scientz, China). The period was 2.0 s with a 2.0-s interval in an ice-water bath for 5 min, unless otherwise indicated. No bacterial colonies were observed in a plate test (15 g/L agar in chloride-free medium), which suggested that the *E. coli* cells were completely disrupted by the high-intensity ultrasound.

The CIP antibiotic in both extracted biofilms and disrupted *E. coli* cells was treated with a vacuum freeze-drying technique (−65 °C) that was followed by extraction using acetonitrile (7.0 mL) with a 1% formic acid-water solution (0.5 mL) (Johnston et al., 2002). The solutions were processed in a vortex mixer for 6 min and then centrifuged at 6000 *g* and 4 °C. This process was performed thrice, and the supernatants were pooled for later chromatographic analysis. The CIP in the supernatant was analyzed by high-performance liquid chromatography (HPLC) in an instrumental setup that included a 20-mL automatic liquid sampler, a Zorbax XDB-C18 column (Agilent, USA), and a fluorescence detector (FLD) (1260 series: Agilent, USA). The composition of the mobile phase was constant 87/13, v/v, acetonitrile/aqueous H_3PO_4 buffer (0.025 mmol/L, pH 3.0, adjusted with triethylamine). The FLD was operated at 278-nm excitation and 440-nm emission. The experiment demonstrated that the sequential method, including the CIP extraction and HPLC analysis, gave a high recovery of approximately 98 ± 3.5%, indicating no loss or metabolism of CIP in the static suspension experiments.

After the static suspension experiment, another independent experiment was performed to investigate *E. coli* growth. A portion of *E. coli* from the static suspension experiment was inoculated into fresh chlorine-free medium (40 mL, 4.0×10^7 cells/mL) and incubated for 18 h at 37 °C and 160 rpm. The cell densities (reflecting *E. coli* growth) were determined by a calibration curve for optical density [cell density (cell/mL) = $(1.89 \times OD_{600nm} - 0.01) \times 10^8$], as described in a previous study (Kang et al., 2014).

2.4. Spectroscopic analyses of alkali–earth–metal bridges

CLSM technology was used to observe *in situ* the enhanced FQA–biofilm association via metals. A water-immersion lens (1000×) was used to observe the sample (50 μL) on a slide. Image stacks were created with a Zeiss LSM510 META that was controlled with AIM software (Jena, Germany). The fluorescence signal of the CIP was recorded with an excitation/emission matrix of 278/440 nm. The fluorescence signal of biofilms at this excitation/emission matrix could not be detected, but the signal from CIP attached to biofilms was clearly visible. XPS analysis was performed to probe the Ca2p and Mg2p signals from the bridges that were formed in *E. coli* biofilms (Thermo, USA). The sampling depth was less than 10 nm, suggesting that the sampling site was located in the biofilms and not on the cells (the biofilm thickness was approximately 135 nm).

TEM was used to observe the removal of the biofilm matrix from the *E. coli* surface. Dried *E. coli* cells were placed onto carbon-coated copper grids for TEM observation with a brightfield detector on a JEM-2100 (Tokyo, Japan). Additionally, after the static suspension experiment, the CIP-containing biofilms that had been extracted from the *E. coli* surface were also dried at −65 °C. FTIR (Bruker, USA) and ^{13}C NMR (Bruker, Germany) analyses were performed to characterize the functional groups of these dried biofilms through using previous method (Kang et al., 2014; Kang and Zhu, 2013).

2.5. Fluorescence micro titration

Three-dimensional excitation-emission matrix (3DEEM) fluorescence spectroscopy combined with micro titration (Kang et al., 2010, 2015) was used to quantitatively explore the association of FQA with the amino acid residues of biofilms in the presence of alkali–earth metals. In this test, the fluorescence peaks of tryptophan (Trp) residues in biofilms, which were located at 280/340 nm (EX/EM) in the 3DEEM, were traced by continuous microtitration/detection processes (Chen et al., 2003; Kang et al., 2010). Specifically, a $CaSO_4$ or $MgSO_4$ stock solution (10 mmol/L) was added in advance of the 20-mL aqueous biofilm solution (0.5 mg/L, dry weight basis) to obtain a 250 μmol/L Ca^{2+} or Mg^{2+} solution. Afterwards, an aqueous CIP stock solution (10 μmol/L) was titrated into each aqueous biofilm solution containing Ca^{2+} or Mg^{2+} using a chromatographic injector (25-μL scale, Agilent, Santa Clara, CA, USA); this step was followed by magnetic stirring for 20 min at 160 rpm, pH 7.0, and 25°C. The fluorescence spectrum was recorded at an excitation wavelength of 200–370 nm (5-nm bandwidth) and an emission wavelength of 280–500 nm (5-nm bandwidth) at a speed of 3000 nm/min (F96PRO, Lengguang). These microtitration/detection procedures were repeated until there was no significant change in the fluorescence intensity. To obtain comparative data, similar procedures were also performed to explore the association between CIP and the biofilm matrix in the absence of alkali–earth metals. The fluorescence peak from extracellular biofilms matrix (EX/EM: 280/340 nm) did not overlap with the FQA peak (EX/EM: 278/440 nm). Thus, the changes in the fluorescence intensity of Trp residues in the biofilms that were caused by the CIP antibiotic could be well described by the relationship between the fluorescence intensity and the quencher concentration (Boaz and Rollefson, 1950; Eftink, 1997; Lakowicz and Weber, 1973). The Stern–Volmer equation is given as follows (Valeur and Berberan-Santos, 2012):

$$\frac{F_0}{F} = 1 + K_q \tau_0 [Q] = 1 + K_{SV}[Q] \quad (1)$$

where F_0 and F are the relative fluorescence intensity of the

chromophore in the absence and presence of the quencher, respectively; K_q is the bimolecular quenching rate constant; τ_0 is the average lifetime of the fluorophore in the absence of the quencher; [Q] is the concentration of the quencher; and K_{SV} is the Stern–Volmer quenching constant. For the static quenching process, equation (2) was used to determine the association constant (K_A) and the number of binding sites (n) (Bi et al., 2004). The association constants with biofilms via metal bridging were determined for all eight FQAs as follows:

$$\log[(F_0 - F)/F] = \log K_A + n \log[Q]. \quad (2)$$

2.6. Quantum mechanical/molecular mechanical (QM/MM) modeling

Utilizing Gabedit software (Version 2.4.5) (Allouche, 2011), we structured the 20 standard amino acid residues: alanine, leucine, isoleucine, valine, proline, phenylalanine, methionine, tryptophan, glycine, serine, glutamine, threonine, cysteine, asparagine, tyrosine, aspartic acid, glutamic acid, lysine, arginine, and histidine. These residues were docked with the CIP antibiotic via an alkali–earth–metal bridge. The key bridging site in biofilms must meet two necessary conditions: a high abundance in biofilms and a high bridging energy between the residue-metal and the FQA. First, the backbones of oligopeptides were composed of the reported seven most common amino acids in bacterial biofilms (Phe, Gly, Asn, Gln, Ser, Thr, and Tyr) (Nakashima and Nishikawa, 1992, 1994). The 20 standard amino acid residues (R) were then successively joined in pairs to both sides of these backbones to structure the amino and carboxyl termini (NH_2-R-Phe-Gly-Asn-Pro-Gln-Ser-Thr-Tyr-R-COOH). This unified model contains 20 short-chain polypeptides (4940 atoms in all) that share a common central sequence and sample the 20 different amino acid residues at each end. Second, the highest bridging energy between the Trp-metal and the FQA was determined on the basis of the QM/MM computation. Additionally, the wave functions from the computation were analyzed using the Multiwfn program. Bridging energies for the combination of Trp with each of the eight FQAs via a metal girder were computed based on a frequency analysis from the "FQA–Ca/Mg–Trp residue" model.

Our own multilayered, N-layered integrated molecular orbital and molecular mechanics (ONIOM) scheme in Gaussian 09 was used to conduct the combined QM/MM computation (Dapprich et al., 1999; Trucks et al., 2009). The entire molecular system was partitioned into two layers: a QM system (CIP–metal–residue), which was treated with a high-level method, and an MM system, consisting of the peripheral molecular system (backbone of oligopeptides), which was treated with a low-level method. In this study, the MM system, as described by the Assisted Model Building with Energy Refinement (AMBER) force field (Cornell et al., 1995), consisted of the peripheral protein structures but excluded the CIP antibiotic, the metal girder, and the 20 amino acid residues. The QM system consisted of the CIP antibiotic, the metal girder, and the amino acid residues that were involved in the bridging reaction. The density function B3LYP was used to treat the QM model system. The geometries of the model system were optimized with the 6-31G(d, p) basis set (Petersson and Al-Laham, 1991; Petersson et al., 1988) with a long-range correction of DFT-D3 (Trucks et al., 2009). All of the atoms in both layers were free to move in the geometry optimization calculations. A Trp residue was determined as a major bridging site. The bridging energies at Trp residue-metals were determined for all eight FQAs. Solvent (water) effects were implicitly taken into consideration in all computations.

2.7. Bonding type and bridging energy

The wave functions from the computation were analyzed by the Multiwfn program (Lu and Chen, 2012). Many pieces of information were extracted by this software, including the reduced density gradient (RDG), the bridging energy, and the Lorentz oscillator. The Lorentz oscillators were used to predict the FTIR spectra, which were then compared with our experimental results. The bridging site at the Trp residue predicted by the FTIR computation was confirmed with the experimental FTIR, which supported the reliability of the model. Based on the functions of the CIP–metal–Trp residue combination, a topological analysis and a graphic illustration of the distribution of the electron density were also performed using the Multiwfn program (Lu and Chen, 2012). The theoretical method for the discrimination of different bonding types can be explained by the quantum mechanical electron density ($\rho(r)$) (Johnson et al., 2010; Kang et al., 2015):

$$\mathrm{RDG}(r) = \frac{1}{2(3\pi^2)^{1/3}} \frac{|\nabla\rho(r)|}{\rho(r)^{4/3}}, \quad (3)$$

where $\rho(r)$, $|\nabla\rho(r)|$, and ∇ are the quantum mechanical electron density, the gradient operator, and the modular arithmetic of the gradient operator for the quantum mechanical electron density, respectively. The bonding types were identified and drawn with interactive isosurfaces around the metal bridge. In the colored contour planes between atoms, we used different colors to represent the bonding types between the metal and the CIP/residue. Blue, green and, red were used to represent strong coordinate bonds, weak vdWs bonds, and intermolecular repulsion, respectively. The bridging energies for the combination of Trp with each of the eight FQAs via a metal girder were computed based on a frequency analysis from the "FQA–Ca/Mg–Trp residue" model. The calculation was as follows:

$$\text{Bridging energy } (\Delta G) = G_{\mathrm{FQA-metal\cdots Trp}} - \left(G_{\mathrm{FQA-metal}} + G_{\mathrm{Trp}}\right), \quad (4)$$

where $G_{\mathrm{FQA\text{-}metal\cdots Trp}}$, $G_{\mathrm{FQA\text{-}metal}}$, and G_{Trp} are the Gibbs free energies (G) of the FQA-metal···Trp (dotted line represents the docking point), the FQA-metal bridge head, and the Trp residue in the polypeptide, respectively.

3. Results and discussion

3.1. Interactions of a model FQA, CIP, with biofilms are enhanced by a metal bridge

Fig. 1a–d presents a group of CLSM images that demonstrate the metal-enhanced CIP-biofilm association on the surface of *E. coli*. In the absence of alkali–earth metals and CIP, a fluorescence signal was not observed, as is apparent in Fig. 1a. After the addition of only CIP (1.25 μmol/L), some faint and scattered rods are visible in Fig. 1b, indicating a weak association of CIP with *E. coli* biofilms. In the presence of the CIP antibiotic (1.25 μmol/L) and alkali–earth Ca^{2+} (2.0 mmol/L), many bright rods are visible in Fig. 1c, suggesting the Ca^{2+}-enhanced attachment of CIP molecules to extracellular biofilms. Similarly, evidence from the CIP (1.25 μmol/L) and alkali–earth Mg^{2+} (2.0 mmol/L) conditions reveals numerous bright rods (Fig. 1d), confirming the Mg^{2+}-enhanced attachment. These results confirm that alkali–earth metals can enhance the association of CIP with biofilms.

Fig. 1e and f presents the core-level Ca2p and Mg2p signals from XPS, respectively. In the reference $CaSO_4$ sample, the $Ca2p_{3/2}$ and

Please cite this article in press as: Kang, F., et al., Alkali–earth metal bridges formed in biofilm matrices regulate the uptake of fluoroquinolone antibiotics and protect against bacterial apoptosis, Environmental Pollution (2016), http://dx.doi.org/10.1016/j.envpol.2016.09.029

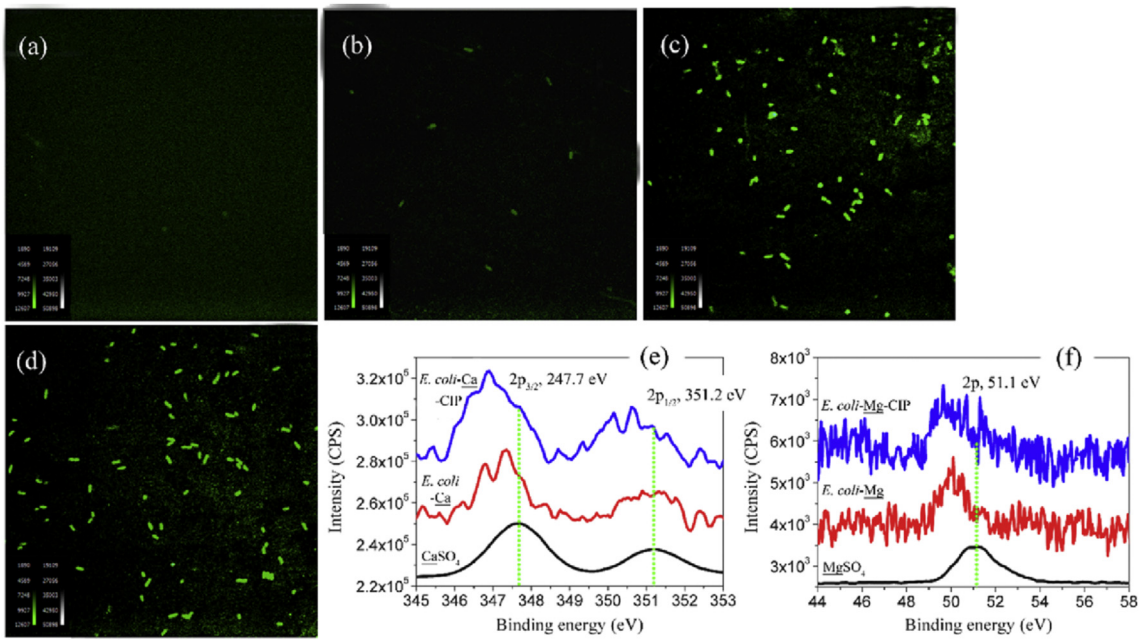

Fig. 1. *In situ* CLSM and corresponding XPS analyses of an alkali–earth–metal bridge formed in *E. coli* biofilms. (a): *E. coli* alone. (b): *E. coli* plus ciprofloxacin (CIP). (c): *E. coli* plus Ca^{2+} and CIP. (d): *E. coli* plus Mg^{2+} and CIP. XPS analyses of a Ca^{2+} bridge (e) and a Mg^{2+} bridge (f). The density of *E. coli* was approximately 1.0×10^8 cells/mL. The concentrations of the alkali–earth metals and CIP were 2.0 mmol/L and 1.25 μmol/L, respectively.

$Ca2p_{1/2}$ peaks were located at 347.7 and 351.2 eV, respectively. After the addition of Ca^{2+} to aqueous *E. coli*, $Ca2p_{3/2}$ produced two peaks (primary 347.25 eV and secondary 346.7 eV; Fig. 1e) that shifted towards a lower energy by 0.45 and 3.95 eV, respectively. The $Ca2p_{1/2}$ peak shifted towards a lower energy by 0.1 eV. As CIP (1.25 μmol/L) was subsequently added, the signal continuously shifted towards a lower energy, from a primary peak ($Ca2p_{1/2}$) of 350.6 eV and a secondary peak of 350.3 eV to lower primary (346.8 eV) and secondary peaks (346.4 eV; shoulder peak). The signal continuously shifted towards a lower energy, indicating that Ca^{2+} acted as an electron acceptor and attracted redundant electrons from the electron-donating biofilms and CIP (Gosselink et al., 2012; Stipp and Hochella, 1991). Combined with the CLSM result, these findings indicate that the Ca^{2+}-enhanced association of CIP with biofilms on the surface of *E. coli* occurs through an alkali–earth Ca^{2+} bridge. Additionally, the Mg2p peak decreased to 50.2 eV when biofilms were added and further decreased to 49.7 eV upon subsequent CIP addition in comparison to the reference sample, $MgSO_4$ (51.1 eV) (Fig. 1f). Overall, the XPS peaks of alkaline-earth metals, mediated by biofilms (Fig. 1e and f) and CIP (Fig. S4), shifted towards a lower energy, demonstrating that the CIP–biofilm association is enhanced by alkali–earth metals and is related to the formation of a metal bridge between them.

3.2. Bridging site in biofilms

The CIP-to-biofilm connection via a metal bridge was analyzed by FTIR spectroscopy (black plots) to further explore the bridging site in biofilms. In the FTIR spectrum of biofilm alone (Fig. 2a), the stretching vibrations of the C=O band at 1675 cm^{-1} and N–H bending and C–N stretching vibrations at 1600 ± 10 cm^{-1} are related to amino acid residues or peptides from proteins in extracellular biofilms. The band at 1430 cm^{-1} denotes the stretching vibration of C–OH in carboxylates (Byler and Susi, 1986; Deacon and Phillips, 1980), whereas the bands near 1115 and 1010 cm^{-1} are ascribed to the stretching vibrations of hydroxyl and C–O–C in saccharides, respectively (Kang and Zhu, 2013). After the binding of CIP via Ca^{2+} (Fig. 2b) and Mg^{2+} bridges (Fig. 2c), the characteristics of the C=O band at 1675 cm^{-1} became weaker compared with those of biofilms alone (Fig. 2a), suggesting that carbonyl groups in the amino acid residues of extracellular biofilms are responsible for the formation of the metal bridge. The band at 1430 cm^{-1}, which is related to C–OH in carboxylates, also became much weaker (Fig. 2b and c). Considering the change in the C=O band at 1675 cm^{-1}, these results suggest that the carboxylates in the amino acid residues of biofilms are responsible for the alkali–earth–metal bridges.

Fig. 2a–c shows a group of computational FTIR spectra (red plots) that were plotted by the Lorentz oscillator (blue plots) based on computation from short polypeptides. After associating Trp carboxyl groups with CIP via Ca^{2+} (Fig. 2b) or Mg^{2+} (Fig. 2c), the bands at 1675 and 1430 cm^{-1} became weaker (decrease in molar absorption coefficients). These results further confirm that carboxyl groups of structured Trp residues may act as the main bridging sites associated with the formation of alkali–earth–metal bridges in biofilms (further analysis in Fig. 5). In this study, contribution of COOH in humics to the bridging may be ruled out, because humic and fulvic acids were not observed in the highly sensitive three-dimensional excitation-emission matrix (3DEEM) spectra (Fig. S1), which may be attributed to the lack of long-term humification (Milori et al., 2002).

CIP-to-biofilm associations via metal bridges may be further analyzed by the ^{13}C NMR spectral fingerprints of biofilms (Fig. 2d). Based on previous work (Wishart et al., 1995), the carboxyl groups in biofilms may be assigned to Trp (176.1 ppm), Tyr (175.8 ppm), Phe (175.7 ppm), Gly (174.9 ppm), Thr (174.7 ppm), Ser (174.4 ppm), Cys (oxidized and reduced states, 174.6 ± 0.2 ppm), and His (174.0 ppm) residues. In Fig. 2d, resonance intensity of Trp residues (176.1 ppm) was dominant in all peaks; a comparison of this signal with different treatments revealed a marked downfield shift ($\Delta\delta = 0.2$) of the resonances attributed to the carbon signals of carboxyl residues in biofilms after treatment of biofilms with Mg/Ca-CIP. The downfield shift indicates that there are some

Please cite this article in press as: Kang, F., et al., Alkali–earth metal bridges formed in biofilm matrices regulate the uptake of fluoroquinolone antibiotics and protect against bacterial apoptosis, Environmental Pollution (2016), http://dx.doi.org/10.1016/j.envpol.2016.09.029

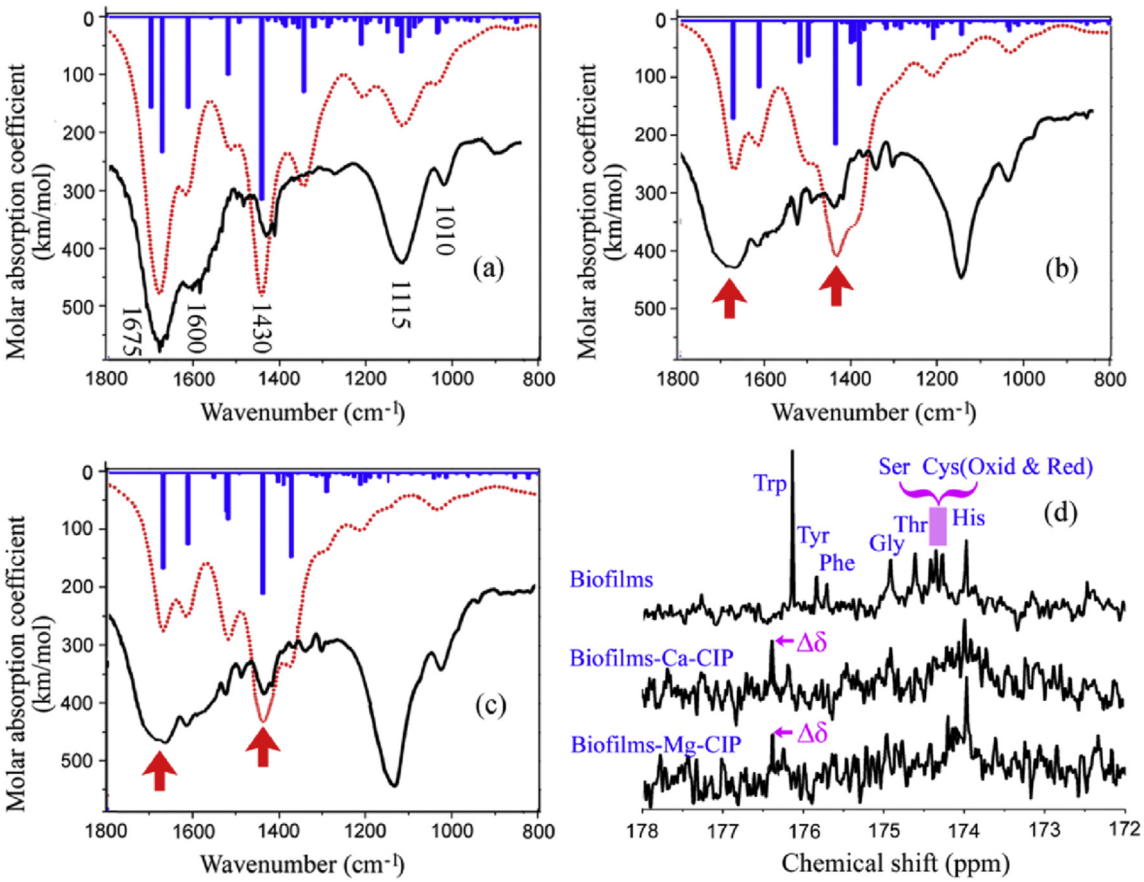

Fig. 2. FTIR and ^{13}C NMR spectra of biofilms before and after their association with CIP via alkali–earth Ca^{2+} and Mg^{2+} bridges. FTIR spectra: (a) biofilm alone; (b) biofilm-Ca^{2+}-CIP; (c) biofilm-Mg^{2+}-CIP. Black plots represent the experimental data. Blue bar charts and red plots represent the Lorentz oscillators and infrared (IR) spectra from the computation at the B3LYP/6-31G(d, p) level with a dispersion-corrected DFT-D3(BJ). Red arrows represent the absorption bands related to the bridging sites. (d) Experimental ^{13}C NMR spectra from biofilm, biofilm-Ca^{2+}-CIP, and biofilm-Mg^{2+}-CIP. After the combination of biofilms with Mg/Ca-CIP, the two pink arrows represent two marked downfield shifts ($\Delta\delta = 0.2$) of the resonances that are attributed to the carbon signal of the carboxyl residues in biofilms. (For interpretation of the references to colour in this figure legend, the reader is referred to the web version of this article.)

multinuclear species containing calcium/magnesium ions that are bridged through the carboxylates of Trp (Barszcz et al., 2013), as Trp residues exhibited the highest abundance and the most obvious change in all of the resonance signals.

3.3. Trans-biofilm uptake of FQA

Fig. S2 shows the appearance of *E. coli* before and after biofilm manipulation, suggesting the removal of biofilms from the surface of low-biofilm *E. coli*. Fig. 3a shows that the concentration of CIP that was retained in high biofilms (135-nm thick in Fig. S2) increased from $(5.2 \pm 0.3) \times 10^{-3}$ to 2.1×10^{-2} μmol/10^9 cells as Ca^{2+} was added at concentrations up to 3.5 mmol/L. However, the concentration of CIP in low biofilms increased only from $(5.2 \pm 0.3) \times 10^{-3}$ to 1.56×10^{-2} μmol/10^9 cells. High biofilms on the *E. coli* surface caused greater retardation of CIP in the extracellular matrix. Fig. 3a also shows that, in contrast, the intracellular CIP concentration in high-biofilm *E. coli* gradually decreased from $(4.0 \pm 0.2) \times 10^{-3}$ to 2.5×10^{-3} μmol/10^9 cells when Ca^{2+} was added at concentrations up to 3.5 mmol/L. The intracellular CIP concentration in low-biofilm *E. coli* decreased to 3.7×10^{-3} μmol/10^9 cells with Ca^{2+} addition, but this value was still greater than that in high-biofilm *E. coli*. These findings confirm that extracellular retardation in biofilms, which is enhanced by alkali–earth–Ca^{2+} bridges, reduces cellular uptake of the CIP antibiotic.

Fig. 3b presents that with the addition of alkali–earth Mg^{2+} (0–3.5 mmol/L), the concentration of CIP that was retained in high biofilms on the surface of *E. coli* increased from $(5.5 \pm 0.5) \times 10^{-3}$ to 2.9×10^{-2} μmol/10^9 cells, whereas the concentration in low biofilms increased less, from $(5.5 \pm 0.5) \times 10^{-3}$ to 1.8×10^{-2} μmol/10^9 cells. Correspondingly, the intracellular CIP concentration in low-biofilm *E. coli* decreased to a final value of 2.7×10^{-3} μmol/10^9 cells, which was slightly higher than that in high-biofilm *E. coli* (2.4×10^{-3} μmol/10^9 cells). Similar findings reconfirm that high biofilms on bacterial surfaces, which are enhanced by the formation of alkali–earth–metal bridges, restrict the cellular uptake of CIP.

Fig. 3c shows the trans-biofilm transport rate of CIP into cells (r) with the addition of alkali–earth metals. As the Ca^{2+} concentration increased up to 3.5 mmol/L (CIP = 1.25 μmol/L), the r value for high-biofilm *E. coli* decreased from $(2.06 \pm 0.02) \times 10^{-4}$ to 1.09×10^{-4} μmol/μm^2 h 10^9 cells. In the low-biofilm *E. coli*, the r value was reduced from $(2.06 \pm 0.02) \times 10^{-4}$ to 1.75×10^{-4} μmol/μm^2 h 10^9 cells. High biofilms act to lower the trans-biofilm transport rate of CIP, and alkali–earth–metal bridges formed in high biofilms will have greater potential for decreasing trans-biofilm antibiotic transport. In the presence of Mg^{2+} (0–3.5 mmol/L), the r value was reduced from $(2.10 \pm 0.01) \times 10^{-4}$ to 1.31×10^{-4} μmol/μm^2 h 10^9 cells in high-biofilm *E. coli* and to $(2.10 \pm 0.01) \times 10^{-4}$ μmol/μm^2 h 10^9 cells in low-biofilm *E. coli*. This finding further supports the notion that the alkali–earth–metal

Please cite this article in press as: Kang, F., et al., Alkali–earth metal bridges formed in biofilm matrices regulate the uptake of fluoroquinolone antibiotics and protect against bacterial apoptosis, Environmental Pollution (2016), http://dx.doi.org/10.1016/j.envpol.2016.09.029

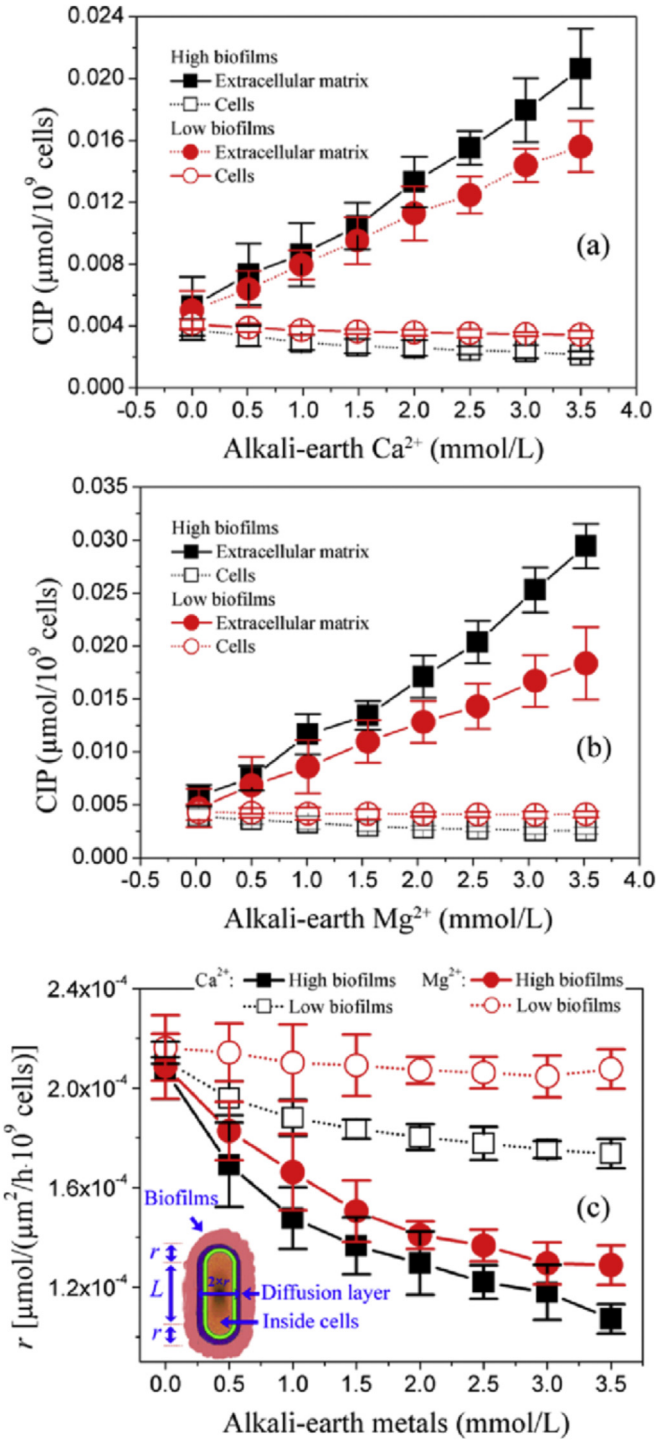

Fig. 3. Extracellular retardation and cell uptake of CIP and its trans-biofilm transport rate (r) in high- and low-biofilm *E. coli*. (a) Ca^{2+}-affected retardation and uptake. (b) Mg^{2+}-affected retardation and uptake. (c) Trans-biofilm transport rate of CIP as a model FQA (r). In (a) and (b), the CIP concentration and cell density were initially 1.25 μmol/L and 1.0×10^8 cells/mL, respectively. In (c), the trans-biofilm transport rate of CIP (r) was calculated based on $r = q/(S \times h)$, where S, q, and h are the interfacial area between bacterial cells and the biofilm layer, the cellular uptake of CIP, and the statically suspension time (4 h), respectively. The superficial area of *E. coli* at the diffusion layer ($S = 2\pi r \times (L + 2\pi r)$) was calculated by randomly selecting 100 *E. coli* cells (diagram at the bottom-left corner of panel (c)). L and r are the length of the rod (subtraction of rod-head cabochons) and the radius of the rod head, respectively ($\pi = 3.14$). The diffusion layer was measured by TEM analysis (average value: 4.95 ± 0.31 μm^2/cell). Error bars represent standard deviations calculated from triplicate samples.

bridges formed in high biofilms are not as conducive to the trans-biofilm transport of CIP. These comparable results regarding extra- and intra-cellular distribution underline an important role for the alkali–earth–metal bridges in reducing the cellular uptake of FQAs.

On the basis of the extra- and intra-cellular distribution in Figs. 3 and 4 depicts the association of *E. coli* growth with the distribution of CIP. In presence of alkali–earth Ca^{2+} (0–3.5 mmol/L, initially added CIP = 1.25 μmol/L), the *E. coli* density was enhanced to 0.42×10^9 cells/mL for high-biofilm manipulation (retardation: 2.08×10^{-2} μmol CIP/10^9 cells; uptake: 2.13×10^{-3} μmol CIP/10^9 cells) and to 0.359×10^9 cells/mL for low-biofilm manipulation (retardation: 1.58×10^{-2} μmol CIP/10^9 cells; uptake: 3.49×10^{-3} μmol CIP/10^9 cells) (Fig. 4a and b). The highest growth density corresponded to the highest extracellular retardation and the lowest cellular uptake of CIP, which demonstrates that the formation of Ca^{2+} bridges on the surface of *E. coli* has a positive effect on the protection of *E. coli* cells. In the presence of alkali–earth Mg^{2+} (0–3.5 mmol/L, initially added CIP = 1.25 μmol/L), *E. coli* densities were enhanced to maximal levels of 0.388×10^9 cells/mL for high-biofilm *E. coli* and 0.365×10^9 cells/mL for low-biofilm *E. coli* (Fig. 4c and d). Accordingly, the CIP retardation values were 0.392×10^{-2} (high biofilms) and 0.365×10^{-2} μmol CIP/10^9 cells (low biofilms), which corresponded to uptake values of 2.58×10^{-3} and $(4.08–4.18) \times 10^{-3}$ μmol CIP/10^9 cells, respectively. The high-biofilm *E. coli* causes a higher density than the low-biofilm *E. coli*. These results lead us to conclude that the formation of a metal bridge in biofilms facilitates *E. coli* growth by enhancing extracellular retardation of CIP.

3.4. Bond types at key sites

Fig. 5a presents results for structured short polypeptides on the basis of the quantum mechanical/molecular mechanical (QM/MM) computation. Metal girder-centered local images are presented in Fig. 5b, d, and f. The electronegative carbonyl groups in FQAs interact with the carboxyl groups of Trp residues in extracellular biofilms through metal girders. To intuitively observe the bond types of the alkali–earth–metal bridges, we analyzed the gradient isosurfaces of the interactive forces around the central alkali–earth metal girder (Fig. 5b, d, and f). The corresponding plots of the reduced density gradient (RDG) versus the electron density multiplied by the sign of the second Hessian eigenvalues are presented in Fig. 5c, e, and g (Johnson et al., 2010). In the absence of metals, the gradient isosurfaces exhibited a rich H-bonding interaction between CIP and biofilms (Fig. 5b). Two pairs of H bonds were observed, between a Trp residue in the biofilm and the carbonyl in the carboxyl of CIP and between the carbonyl of a Trp residue in the biofilm and a hydrogen in pyridine. The corresponding plots of the RDG versus the electron density multiplied by the sign of the second Hessian eigenvalues revealed two spikes, as noted in Fig. 5c (−0.01 to −0.04 au). a spike denoting their attraction (−0.03 to −0.04 au) corresponds to H bonding between a Trp residue in biofilm and the carbonyl of the carboxyl group in CIP. Another spike, at −0.01 to −0.02 au, shows the H bond between a carbonyl in the Trp residue of a biofilm and a hydrogen atom in pyridine. Additionally, a spike at 0 to −0.01 au reveals a weak intramolecular H bond between the pyridine and carbonyl in the molecular interior of the CIP antibiotic. These observations were consistent with previously simulated result from molecular docking between NOR and protein (Lu et al., 2010), suggesting that the CIP–biofilm interaction is based primarily on H bonds.

The gradient isosurfaces exhibited a rich visualization of n–metal electron donor–acceptor (n–metal EDA) interactions (Fig. 5d). Four planar isosurfaces (blue) indicate a strong attraction

Please cite this article in press as: Kang, F., et al., Alkali–earth metal bridges formed in biofilm matrices regulate the uptake of fluoroquinolone antibiotics and protect against bacterial apoptosis, Environmental Pollution (2016), http://dx.doi.org/10.1016/j.envpol.2016.09.029

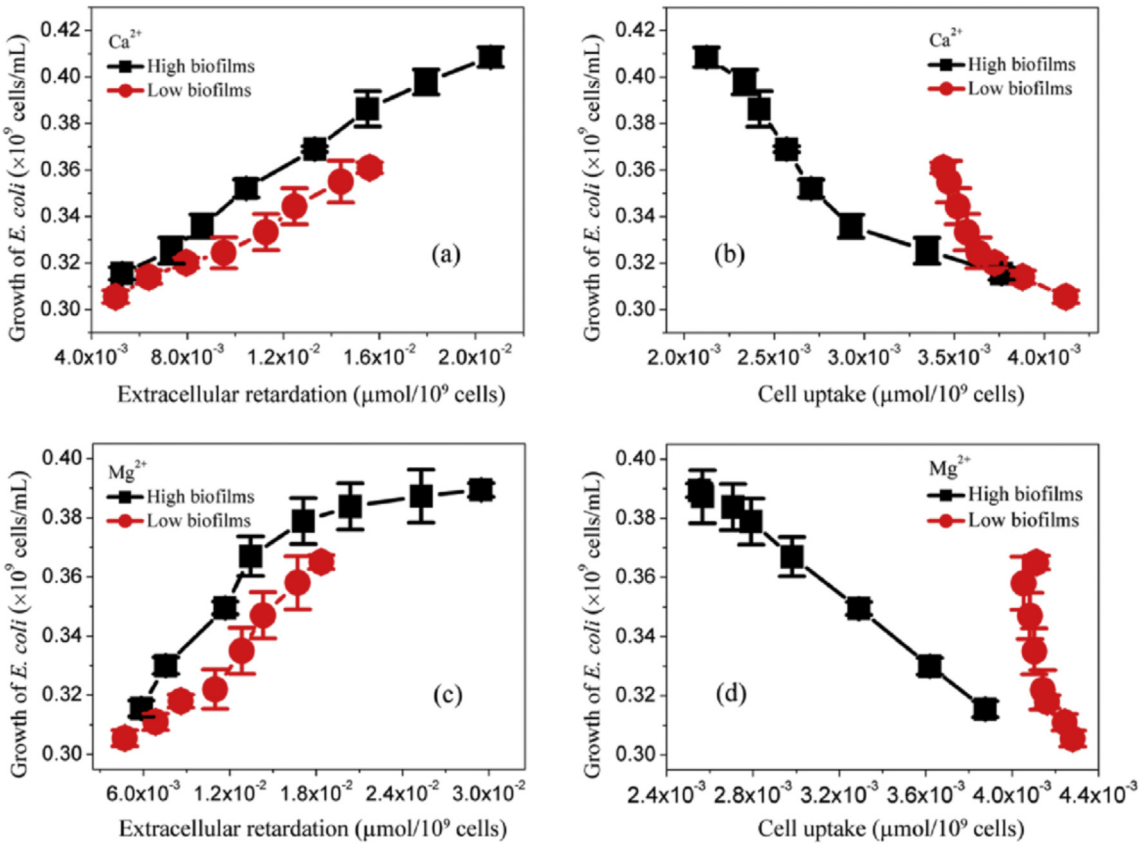

Fig. 4. Association of *E. coli* growth with extracellular retardation and cellular uptake of CIP. After a static suspension experiment (4 h), a portion of the bacterial culture was analyzed to obtain the extracellular retardation and cellular uptake of CIP, while another portion was incubated in fresh LB medium for 18 h to obtain a final *E. coli* density. The data for the extracellular retardation and cellular uptake of CIP antibiotic in the abscissa of the graphs can be found in Fig. 3a–d. The initial concentrations of the added alkali–earth metals ranged from 0 to 3.5 mmol/L. Each data point shown in the figures is the average of three measurements.

between Ca^{2+} and oxygen atoms. The non-bonded interaction between a pair of oxygen atoms in Trp residues, which is also indicated by the red isosurface, shows the repulsion between them. On the CIP side (the left side of Fig. 5d), both of the oxygen atoms in the deprotonated carboxyl group and its adjacent carbonyl in the aromatic nucleus together contacted the Ca^{2+}-bridge girder through a blue oval-shaped gradient isosurface, indicating a strong *n*–metal EDA attraction. On the biofilm side (the right side of Fig. 5d), a pair of oxygen atoms in a deprotonated carboxyl group of a tryptophan residue were associated with a Ca^{2+}-bridge girder through another blue oval-shaped gradient isosurface, further confirming the presence of another strong *n*–metal EDA interaction. These results suggest that both carbonyl/deprotonated carboxyl groups in FQAs and deprotonated carboxyl groups in Trp residues are collectively responsible for the formation of alkali–earth–metal bridges.

Fig. 5e shows plots of RDG versus electron density multiplied by the sign of the second Hessian eigenvalue (corresponding to Fig. 5d). Three low-gradient spikes, at 0.01–0.04 au, indicated molecular repulsions between a pair of oxygen atoms in the deprotonated carboxyl group of a Trp residue and between the carbon of the carboxyl and its adjacent carbon in the aromatic nucleus of CIP (corresponding to the red color of the gradient isosurfaces in Fig. 5d). The spike at −0.018 au revealed the weak vdWs attraction between one of the oxygen atoms in a deprotonated carboxyl group and its adjacent carbonyl in the CIP molecule (corresponding to the green color of the gradient isosurfaces in Fig. 5d). A pair of spikes (−0.03~ −0.06 au) revealed the strong *n*–metal EDA attractions around the alkali–earth–metal bridge girder.

In addition to the weak vdWs attraction in the molecular interiors of CIP and Trp residues, a strong EDA attraction around the central Mg^{2+} girder was also indicated by the visual gradient isosurfaces (Fig. 5f). In Fig. 5g, an apparent low-gradient spike, which corresponds to the isosurface of an Mg^{2+} bridge, has a more negative value at −0.057 a.u, suggesting a stronger EDA interaction of electronegative oxygen atoms with Mg^{2+} than with Ca^{2+}. This quantitative result showing the greater negativity of sign $(\lambda_2)\rho$ suggests that a stronger EDA interaction via an Mg^{2+} bridge might be better able to detain CIP in the extracellular matrices.

3.5. Dependency on bridging energy

Association constants between FQAs and the biofilm matrix via metals were obtained by a fluorescence micro titration (Fig. S3). Fig. 6a shows that the growth rate of *E. coli* increased linearly along with the enhancement of the association constant between FQAs and the biofilm matrix, which implies that the metal bridge-enhanced FQA–biofilm association protects against bacterial apoptosis. The slopes were 0.03 for Ca^{2+}-enhanced growth and 0.09 for Mg^{2+}-enhanced growth. The growth rate (the vertical coordinate) followed the following order: CIP ≈ LOM > NOR > LVX ≈ ENX ≈ OFX > PEF ≈ FLE for Ca^{2+}, and CIP ≈ NOR > ENX > LOM > OFX > LVX > PEF ≈ FLE for Mg^{2+}.

Plots of changes in the Gibbs free energy (ΔG) computed at a major Trp residue site versus the association constant obtained by fluorescence microtitration ($\log K_A$) were used to further explain the dependence of the bridging energy on the alkali–earth–metal

Please cite this article in press as: Kang, F., et al., Alkali–earth metal bridges formed in biofilm matrices regulate the uptake of fluoroquinolone antibiotics and protect against bacterial apoptosis, Environmental Pollution (2016), http://dx.doi.org/10.1016/j.envpol.2016.09.029

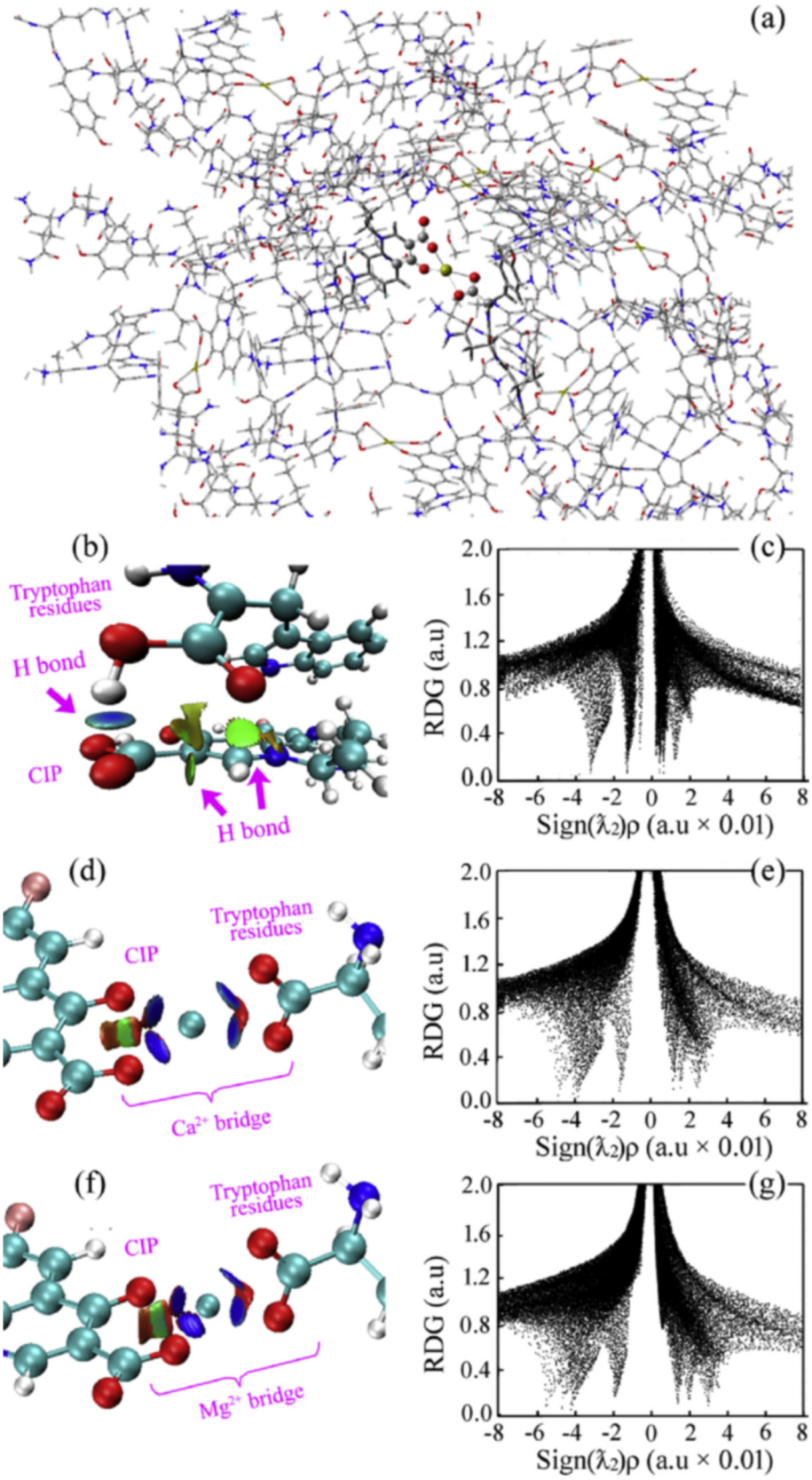

Fig. 5. Models of CIP interactions with Trp residues in biofilms. (a) Model obtained by QM/MM computation of CIP interacting with Trp residues in biofilms via metal bridges. Magnified gradient isosurfaces (b, d, and f) and the corresponding plots of the reduced density gradient versus the electron density multiplied by the sign of the second Hessian eigenvalues (c, e, and g). (b) and (c), CIP-biofilms. (d) and (e), CIP-Ca^{2+}-biofilms. (f) and (g), CIP-Mg^{2+}-biofilms. In (b), (d), and (f), the gradient isosurfaces are colored on a blue-green-red scale according to the values of sign (λ_2)ρ, which range from −0.08 to 0.08 au. Blue, green, and red indicate the strong attraction of an *n*-metal EDA interaction, vdWs interaction, and strong non-bonded overlap, respectively. Here, the sign of λ_2 is used to distinguish bonded ($\lambda_2 < 0$, such as a π−π bonding) from non-bonded ($\lambda_2 > 0$) interactions (a negative value of λ_2 represents strong bonding) (Panels (c), (e), and (g)). The lower the negative value of λ_2, the stronger the attraction in the region. The O, C, H, N, and F in the molecular structures are represented as red, cyan, white, blue, and brown spheres, respectively. Solvent (water) effects were implicitly taken into consideration. (For interpretation of the references to colour in this figure legend, the reader is referred to the web version of this article.)

Please cite this article in press as: Kang, F., et al., Alkali—earth metal bridges formed in biofilm matrices regulate the uptake of fluoroquinolone antibiotics and protect against bacterial apoptosis, Environmental Pollution (2016), http://dx.doi.org/10.1016/j.envpol.2016.09.029

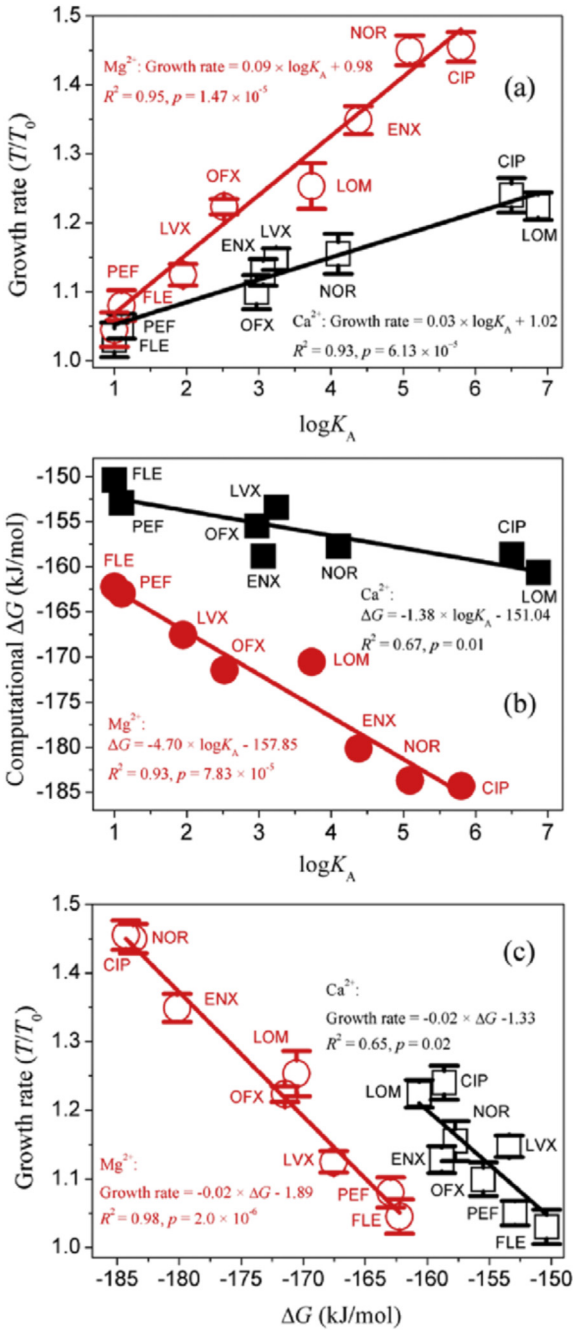

Fig. 6. Correlation of the Trp-Ca···FQA bridging energy at a major tryptophan (Trp) residue site in biofilms (computational $\Delta G_{\text{Trp}\cdots\text{metal-FQAs}}$) with an association constant (K_A, log-transformed) and the rate of *E. coli* growth. (a) Growth rate (T/T_0) versus logK_A. (b) Computed $\Delta G_{\text{Trp}\cdots\text{metal-FQAs}}$ versus logK_A. (c) Growth rate (T/T_0) versus computed $\Delta G_{\text{Trp}\cdots\text{metal-FQAs}}$. The growth rate of *E. coli* was calculated as the ratio of *E. coli* density in the presence of an alkali–earth–metal bridge (T) to the density in the absence of alkali–earth metals (T_0) (growth ratio = T/T_0) after 18 h of incubation with a constant concentration of FQAs (1.25 μmol/L, 37 °C, and 150 rpm). The association constant (logK_A) was obtained by fluorescence microtitration. The Gibbs free energy (ΔG) at the major EDA interaction (Trp···metal-FQ) was computed at the B3LYP/6-31G (d, p) level with a dispersion-corrected DFT-D3 (BJ). The change in ΔG was calculated by the difference between the Trp-metal head and FQ. Solvent (water) effects were implicitly taken into consideration. Each data point shown in panels (a) and (c) is the average of three measurements. R^2: correlation coefficient; p: probability.

bridge (Fig. 6b). It shows the computed ΔG values for the listed eight FQ antibiotics binding at a Trp residue via a metal bridge. A group of strong linear correlations between $\Delta G_{\text{Trp}\cdots\text{Ca-FQAs}}$/$\Delta G_{\text{Trp}\cdots\text{Mg-FQAs}}$ and the corresponding association constants (logK_A) ($R^2 \geq 0.67$; probability, $p \leq 0.01$) were noted. Importantly, a minus sign in the computed ΔG value arises only if a spontaneous reaction occurs. Thus, the linear correlations suggest that higher logK_A values (absolute value) correspond to greater ΔG values. With respect to Mg^{2+} bridging, this plot has a large slope (absolute value of 4.7), suggesting that variations in the FQA-Mg-to-biofilm combination may cause a large change in the bridging energy. All bridging energies were greater than 150 kJ/mol, indicating that all active sites experienced a spontaneously coordinated reaction (Gu et al., 1994), which was associated with EDA interactions.

Fig. 6c shows the linear correlations between ΔG and the rate of *E. coli* growth. Bridging energies combined with FQAs (the horizontal axis) followed a descending order (in abscissa), as follows: FLE ≈ PEF > LVX > OFX > NOR > ENX ≈ CIP > LOM for added Ca^{2+} and FLE ≈ PEF > LVX > OFX ≈ LOM > ENX > NOR ≈ CIP for added Mg^{2+}. With the decrease in ΔG at major n–metal EDA interactions, growth rates exhibit a clear linear reduction. This finding indicates that a weaker CIP–Ca–biofilm combination may result in less retardation, which acts against the growth of *E. coli*. Additionally, the Ca^{2+} and Mg^{2+} bridges had the same slope (−0.02), suggesting that the growth rates of *E. coli* recovered by these two metals are dependent on the bridging energy atTrp residue in biofilms rather than on the particular metal species.

4. Conclusion

More and more attention has been paid to the challenging issue on environmental contamination of antibiotics in recent years. How microbes regulate the trans-biofilm uptake of FQAs is a fundamental question in environmental chemistry and biology. Traditional research thinks basically that bacterially extracellular biofilm matrices are known as passive defense barrier to impede the invasion of hazardous substance, but not know whether FQA attack may be efficiently defused by a metal-reinforced detoxification mechanism occurring at water-biofilm interface. We recently found that metal bridge formed in biofilm matrices anchors the FQAs, and efficiently defuses the FQA attack through this reinforced detoxification mechanism. Here, we present that a deprotonated carboxyl in the tryptophan residues of biofilms acted as a major bridge site, of which one side is a metal and the other is a metal girder jointly connected to the carboxyl and carbonyl of a FQA. Meanwhile, we further demonstrated that a metal bridge formed in extracellular biofilms acts through a suppressive trans-biofilm transport to protect against bacterial apoptosis. Without this metal bridge, extracellular biofilms exhibit higher permeability, larger antibiotic uptake towards cells, and profoundly defective chemotaxis. Computation regarding bridging energy indicates that this metal bridge is favorable for bacterial survival. This new perspective will enhance the understanding of bacterially antibiotic resistance involved in the field of natural products.

Acknowledgment

This work was supported by the National Science Foundation of China (Grant Nos. 41401543, 41502170), the National Science Foundation for Postdoctoral Scientists of China (Grant No. 2014M561662), the Natural Science Foundation of Jiangsu Province of China (Grant Nos. BK20140725), the Fundamental Research Funds for the Central Universities (KJQN201518), and the Special Fund for Agro-Scientific Research in the Public Interest, China (201503107).

Appendix A. Supplementary data

Supplementary data related to this article can be found at http://dx.doi.org/10.1016/j.envpol.2016.09.029.

References

Adkins, J.F., McIntyre, K., Schrag, D.P., 2002. The salinity, temperature, and δ18O of the glacial deep ocean. Science 298, 1769–1773.
Allouche, A.R., 2011. Gabedit-a graphical user interface for computational chemistry softwares. J. Comput. Chem. 32, 174–182.
Aristilde, L., Sposito, G., 2008. Molecular modeling of metal complexation by a fluoroquinolone antibiotic. Environ. Toxicol. Chem. 27, 2304–2310.
Baquero, F., Martínez, J.-L., Cantón, R., 2008. Antibiotics and antibiotic resistance in water environments. Curr. Opin. Biotechnol. 19, 260–265.
Barszcz, B., Masternak, J., Hodorowicz, M., Matczak-Jon, E., Jabłońska-Wawrzycka, A., Stadnicka, K., Zienkiewicz, M., Królewska, K., Kaźmierczak-Barańska, J., 2013. Synthesis, crystal structure and NMR investigation of novel Ca(II) complexes with heterocyclic alcohol, aldehyde and carboxylate ligands. Evaluation of Ca(II) and Cd(II) analogues for anticancer activity. Inorg. Chim. Acta 399, 85–94.
Bi, S., Ding, L., Tian, Y., Song, D., Zhou, X., Liu, X., Zhang, H., 2004. Investigation of the interaction between flavonoids and human serum albumin. J. Mol. Struct. 703, 37–45.
Boaz, H., Rollefson, G., 1950. The quenching of fluorescence. Deviations from the Stern-Volmer law. J. Am. Chem. Soc. 72, 3435–3443.
Bowen, H.J.M., 1979. Environmental Chemistry of the Elements. Academic Press.
Burton, K., 1956. A study of the conditions and mechanism of the diphenylamine reaction for the colorimetric estimation of deoxyribonucleic acid. Biochem. J. 62, 315–323.
Byler, D.M., Susi, H., 1986. Examination of the secondary structure of proteins by deconvolved FTIR spectra. Biopolymers 25, 469–487.
Chen, W., Westerhoff, P., Leenheer, J.A., Booksh, K., 2003. Fluorescence excitation-emission matrix regional integration to quantify spectra for dissolved organic matter. Environ. Sci. Technol. 37, 5701–5710.
Comte, S., Guibaud, G., Baudu, M., 2006. Relations between extraction protocols for activated sludge extracellular polymeric substances (EPS) and EPS complexation properties: part I. comparison of the efficiency of eight EPS extraction methods. Enzyme Microb. Technol. 38, 237–245.
Cornell, W.D., Cieplak, P., Bayly, C.I., Gould, I.R., Merz, K.M., Ferguson, D.M., Spellmeyer, D.C., Fox, T., Caldwell, J.W., Kollman, P.A., 1995. A second generation force field for the simulation of proteins, nucleic acids, and organic molecules. J. Am. Chem. Soc. 117, 5179–5197.
Dapprich, S., Komáromi, I., Byun, K.S., Morokuma, K., Frisch, M.J., 1999. A new ONIOM implementation in Gaussian98. Part I. The calculation of energies, gradients, vibrational frequencies and electric field derivatives. J. Mol. Struct. Thochem 461, 1–21.
Deacon, G., Phillips, R., 1980. Relationships between the carbon-oxygen stretching frequencies of carboxylato complexes and the type of carboxylate coordination. Coord. Chem. Rev. 33, 227–250.
Desnottes, J., Diallo, N., 1992. Cellular uptake and intracellular bactericidal activity of RP 59500 in murine macrophages. J. Antimicrob. Chemother. 30, 107–115.
Dubois, M., Gilles, K.A., Hamilton, J.K., Rebers, P., Smith, F., 1956. Colorimetric method for determination of sugars and related substances. Anal. Chem. 28, 350–356.
Eftink, M.R., 1997. Fluorescence methods for studying equilibrium macromolecule-ligand interactions. Method. Enzymol. 278, 221–257.
Fang, H.H., Xu, L.-C., Chan, K.-Y., 2002. Effects of toxic metals and chemicals on biofilm and biocorrosion. Water Res. 36, 4709–4716.
Gosselink, R.W., van den Berg, R., Xia, W., Muhler, M., de Jong, K.P., Bitter, J.H., 2012. Gas phase oxidation as a tool to introduce oxygen containing groups on metal-loaded carbon nanofibers. Carbon 50, 4424–4431.
Gu, B., Schmitt, J., Chen, Z., Liang, L., McCarthy, J.F., 1994. Adsorption and desorption of natural organic matter on iron oxide: mechanisms and models. Environ. Sci. Technol. 28, 38–46.
Ha, J., Gélabert, A., Spormann, A.M., Brown, G.E., 2010. Role of extracellular polymeric substances in metal ion complexation on *Shewanella oneidensis*: batch uptake, thermodynamic modeling, ATR-FTIR, and EXAFS study. Geochim. Cosmochim. Ac 74, 1–15.
Harvie, C.E., Møller, N., Weare, J.H., 1984. The prediction of mineral solubilities in natural waters: the Na-K-Mg-Ca-H-Cl-SO_4-OH-HCO_3-CO_3-CO_2-H_2O system to high ionic strengths at 25 °C. Geochim. Cosmochim. Ac 48, 723–751.
Johnson, E.R., Keinan, S., Mori-Sanchez, P., Contreras-Garcia, J., Cohen, A.J., Yang, W., 2010. Revealing noncovalent interactions. J. Am. Chem. Soc. 132, 6498–6506.
Johnston, L., Mackay, L., Croft, M., 2002. Determination of quinolones and fluoroquinolones in fish tissue and seafood by high-performance liquid chromatography with electrospray ionisation tandem mass spectrometric detection. J. Chromatogr. A 982, 97–109.
Kang, F., Alvarez, P.J., Zhu, D., 2014. Microbial extracellular polymeric substances reduce Ag^+ to silver nanoparticles and antagonize bactericidal activity. Environ. Sci. Technol. 48, 316–322.
Kang, F., Gao, Y., Wang, Q., 2010. Inhibition of free DNA degradation by the deformation of DNA exposed to trace polycyclic aromatic hydrocarbon contaminants. Environ. Sci. Technol. 44, 8891–8896.
Kang, F., Hu, X., Liu, J., Gao, Y., 2015. Noncovalent binding of polycyclic aromatic hydrocarbons with genetic bases reducing the *in-vitro* lateral transfer of antibiotic resistant genes. Environ. Sci. Technol. 49, 10340–10348.
Kang, F., Zhu, D., 2013. Abiotic reduction of 1, 3-dinitrobenzene by aqueous dissolved extracellular polymeric substances produced by microorganisms. J. Environ. Qual. 42, 1441–1448.
Kolpin, D.W., Furlong, E.T., Meyer, M.T., Thurman, E.M., Zaugg, S.D., Barber, L.B., Buxton, H.T., 2002. Pharmaceuticals, hormones, and other organic wastewater contaminants in US streams, 1999-2000: a national reconnaissance. Environ. Sci. Technol. 36, 1202–1211.
Lakowicz, J.R., Weber, G., 1973. Quenching of fluorescence by oxygen. Probe for structural fluctuations in macromolecules. Biochemistry 12, 4161–4170.
Liu, H., Fang, H.H., 2002. Extraction of extracellular polymeric substances (EPS) of sludges. J. Biotechnol. 95, 249–256.
Lowry, O.H., Rosebrough, N.J., Farr, A.L., Randall, R.J., 1951. Protein measurement with the Folin phenol reagent. J. Biol. Chem. 193, 265–275.
Lu, T., Chen, F., 2012. Multiwfn: a multifunctional wavefunction analyzer. J. Comput. Chem. 33, 580–592.
Lu, Y., Wang, G., Lu, X., Lv, J., Xu, M., Zhang, W., 2010. Molecular mechanism of interaction between norfloxacin and trypsin studied by molecular spectroscopy and modeling. Spectrochim. Acta. A 75, 261–266.
Martínez, J.L., Baquero, F., Andersson, D.I., 2007. Predicting antibiotic resistance. Nat. Rev. Microbiol. 5, 958–965.
Martinez, J.L., 2009. Environmental pollution by antibiotics and by antibiotic resistance determinants. Environ. Pollut. 157, 2893–2902.
Merino, S., Domènech, Ò., Díez, I., Sanz, F., Viñas, M., Montero, M.T., Hernández-Borrell, J., 2003. Effects of ciprofloxacin on *Escherichia coli* lipid bilayers: an atomic force microscopy study. Langmuir 19, 6922–6927.
Merino, S., Vázquez, J.L., Domènech, Ò., Berlanga, M., Viñas, M., Montero, M.T., Hernández-Borrell, J., 2002. Fluoroquinolone-biomembrane interaction at the DPPC/PG lipid-bilayer interface. Langmuir 18, 3288–3292.
Milori, D.M., Martin-Neto, L., Bayer, C., Mielniczuk, J., Bagnato, V.S., 2002. Humification degree of soil humic acids determined by fluorescence spectroscopy. Soil Sci. 167, 739–749.
Mompelat, S., Le Bot, B., Thomas, O., 2009. Occurrence and fate of pharmaceutical products and by-products, from resource to drinking water. Environ. Int. 35, 803–814.
Nakashima, H., Nishikawa, K., 1992. The amino acid composition is different between the cytoplasmic and extracellular sides in membrane proteins. Febs. Lett. 303, 141–146.
Nakashima, H., Nishikawa, K., 1994. Discrimination of intracellular and extracellular proteins using amino acid composition and residue-pair frequencies. J. Mol. Biol. 238, 54–61.
Petersson, G., Al-Laham, M.A., 1991. A complete basis set model chemistry. II. Open-shell systems and the total energies of the first-row atoms. J. Chem. Phys. 94, 6081–6090.
Petersson, G., Bennett, A., Tensfeldt, T.G., Al-Laham, M.A., Shirley, W.A., Mantzaris, J., 1988. A complete basis set model chemistry. I. The total energies of closed-shell atoms and hydrides of the first-row elements. J. Chem. Phys. 89, 2193–2218.
Pruden, A., Larsson, D.J., Amézquita, A., Collignon, P., Brandt, K.K., Graham, D.W., Lazorchak, J.M., Suzuki, S., Silley, P., Snape, J.R., 2013. Management options for reducing the release of antibiotics and antibiotic resistance genes to the environment. Environ. Heal. Perspect. 121, 878–885.
Pruden, A., Pei, R., Storteboom, H., Carlson, K.H., 2006. Antibiotic resistance genes as emerging contaminants: studies in northern Colorado. Environ. Sci. Technol. 40, 7445–7450.
Rice, L.B., 2006. Unmet medical needs in antibacterial therapy. Biochem. Pharmacol. 71, 991–995.
Stipp, S.L., Hochella, M.F., 1991. Structure and bonding environments at the calcite surface as observed with X-ray photoelectron spectroscopy (XPS) and low energy electron diffraction (LEED). Geochim. Cosmochim. Ac 55, 1723–1736.
Sun, X., Wang, S., Zhang, X., Chen, J.P., Li, X., Gao, B., Ma, Y., 2009. Spectroscopic study of Zn^{2+} and Co^{2+} binding to extracellular polymeric substances (EPS) from aerobic granules. J. Colloid Interface Sci. 335, 11–17.
Sundararajan, M., Rajaraman, G., Ghosh, S.K., 2011. Speciation of uranyl ions in fulvic acid and humic acid: a DFT exploration. Phys. Chem. Chem. Phys. 13, 18038–18046.
Trucks, G., Schlegel, H., Scuseria, G., Robb, M., Cheeseman, J., Scalmani, G., Barone, V., Mennucci, B., Petersson, G., Nakatsuji, H., 2009. Gaussian 09, Revision E. 01. Gaussian, Inc, Wallingford, CT.
Turiel, E., Martín-Esteban, A., Tadeo, J.L., 2006. Multiresidue analysis of quinolones and fluoroquinolones in soil by ultrasonic-assisted extraction in small columns and HPLC-UV. Anal. Chim. Acta 562, 30–35.
Valeur, B., Berberan-Santos, M.N., 2012. Molecular Fluorescence: Principles and Applications. John Wiley & Sons.
Walter, H., 2012. Partitioning in Aqueous Two–phase System: Theory, Methods, Uses, and Applications to Biotechnology. Elsevier.
Wingender, J., Neu, T.R., Flemming, H.-C., 2012. Microbial Extracellular Polymeric Substances: Characterization, Structure and Function. Springer Science & Business Media.

Please cite this article in press as: Kang, F., et al., Alkali–earth metal bridges formed in biofilm matrices regulate the uptake of fluoroquinolone antibiotics and protect against bacterial apoptosis, Environmental Pollution (2016), http://dx.doi.org/10.1016/j.envpol.2016.09.029

Wishart, D.S., Bigam, C.G., Holm, A., Hodges, R.S., Sykes, B.D., 1995. ^{1}H, ^{13}C and ^{15}N random coil NMR chemical shifts of the common amino acids. I. Investigations of nearest-neighbor effects. J. Biomol. NMR 5, 67–81.

Xiong, J., Stehle, T., Zhang, R., Joachimiak, A., Frech, M., Goodman, S.L., Arnaout, M.A., 2002. Crystal structure of the extracellular segment of integrin αVβ3 in complex with an Arg-Gly-Asp ligand. Science 296, 151–155.

Xu, W.-h., Zhang, G., Zou, S.-c., Li, X.-d., Liu, Y.-c., 2007. Determination of selected antibiotics in the Victoria Harbour and the Pearl River, South China using high-performance liquid chromatography-electrospray ionization tandem mass spectrometry. Environ. Pollut. 145, 672–679.

Zhang, Q., Zhao, L., Dong, Y., Huang, G., 2012. Sorption of norfloxacin onto humic acid extracted from weathered coal. J. Environ. Manag. 102, 165–172.

Please cite this article in press as: Kang, F., et al., Alkali–earth metal bridges formed in biofilm matrices regulate the uptake of fluoroquinolone antibiotics and protect against bacterial apoptosis, Environmental Pollution (2016), http://dx.doi.org/10.1016/j.envpol.2016.09.029